EFFECT OF CONCENTRATION OF POLYURETHANE ON THE ANTI-CORROSIVE PROPERTY OF CRESOL BASED BENZOXAZINE - ELECTROCHEMICAL AND QUANTUM CHEMICAL APPROACH

C. Usha[1*], M. Sivaraju[2], P. Shanmugasundaram[3]

Abstract

Benzoxazine and polyurethanes were used for the polymer's synthesis based on the cresol moity having monomer. By adjusting the polyurethane content, three copolymers develop, and each one's corrosion inhibition capabilities are investigated. NMR, FT-IR, and UV-visible spectroscopy techniques were first used to characterise the synthesised monomer, which had cresol as its central component. Then, using the same FT-IR and UV-visible spectroscopy, the produced copolymers are examined. Tafel studies are conducted about corrosion inhibition, and the results suggest that co-polymers with increased polyurethane content have higher anti-corrosive capabilities. In addition, studies of the materials' physical characteristics, such as water absorption and gel content, are conducted. Further, the monomer was subjected to a density functional theory calculation, which examines the improved outcomes that are consistent with another experimental research.

Keywords: Cresol, polyurethane, Co-polymer, corrosion inhibition, DFT

[1*,2,3]PG & Research Department of Chemistry, Thiruvalluvar Governement Arts College (Affiliated to Periyar University), Rasipuram, Namakkal – 637401.

***Corresponding Author**:- C.Usha
E-mail : tkr_jai@hotmail.com
*PG & Research Department of Chemistry, Thiruvalluvar Governement Arts College (Affiliated to Periyar University), Rasipuram, Namakkal – 637401.

DOI: 10.53555/ecb/2023.12.Si13.232

Introduction

One of the often-used materials, metal is used in many different fields, such as construction, healthcare, and transportation. [1] Due to its exceptional qualities, mild steel (MS) in particular finds many uses in industry, construction, and daily life. [2] The exposure to MS corrosion, which is thought to cost more than 1.8 trillion USD annually globally, has an impact on the economics of industrialised nations. [3] Additionally, because biomaterials are continually being pushed to their limits by biological fluids, corrosion on MS does have a negative impact on human health, resulting in side effects like inflammation and allergic reactions. [4,5] Scientists therefore confront higher difficulties in reducing corrosion on MS, which is why they are particularly intrigued by organic coatings that might prevent corrosion on the metallic surface. [6-9] Epoxy-based resins have been widely used in recent years as a coating material to restrict the correction of MS because of their processability, excellent chemical resistance, high cross-linking density, and strong adhesion/affinity to substrates. [10-11] But several drawbacks, like a higher water absorption rate and a highly hydroscopic nature, also operate as a barrier to their employment in particle applications. [12-13] Unlike epoxides, phenolic resin allows those who can easily make polymers through conversational heat treatment to do so. [14] Additionally, this kind of polymer studies very significant traits including a less hydrophilic nature, nearly little shrinkage, low surface free energy, and dielectric properties. [15-16] A brand-new variety of thermosetting phenolic resin called polybenzoxazine exhibits the desired properties as well, including high char yield, great heat and chemical resistance, and a very long shelf life. [17] Dichlorophenyl Benzoxazine Monomers (DCB) have also been created using the Mannich condensation reaction between a primary amine, phenol, and formaldehyde. [18] Despite having several advantages because of its limitations, it is limited by its anti-corrosive efficacy, including high curing temperature and brittleness. [19-20] To address this, benzoxazine-based polymers may be functionalized, and polyurethane is one of the best materials with a high level of mechanical stability. [21-22] As a result, the concept of fusing polyurethane with benzoxazine to produce a polymeric substance with the potential for intriguing features has developed. The anti-corrosive properties of the benzoxazine-polyurethane combination have therefore been examined here. Three different polymers have been described by altering the names of the polyurethane ratios 100:60, 100:80, and 100:100 in this line. Materials were examined for corrosion studies, and the synthesised monomer has been studied using NMR, FT-IR, and UV-visible spectroscopy.

Experimental methods

Synthesis of the monomer

The experiment employed a set of substances comprising O-cresol (1g, 6.572 mmol) and 3,5-dichloroaniline. To synthesize the monomer (DCB), a mixture of Paraformaldehyde (0.414g, 13.802) and HCl (6.572 mmol) in $CHCl_3$ (20 mL) was refluxed for 24 hours. The reaction's progress was tracked through thin-layer chromatography. The mixture was then extracted with chloroform (150 mL) and washed with water (100 mL) and brine solution (100 mL) to eliminate water-soluble impurities. The resulting organic layer was separated and dried using anhydrous sodium sulphate to remove any residual water. The chloroform solution obtained was then evaporated under low pressure to produce the DCB monomer. This monomer (DCB) was utilized to create a coating material that contains polyurethane as its polymeric component.

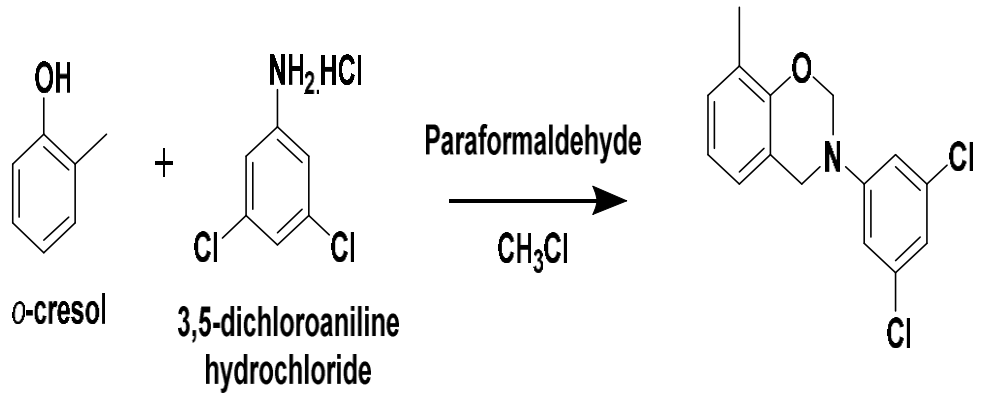

Scheme 1: Chemical synthesis of Dichlorophenyl Benzoxazine monomer

Synthesis of the Dichlorophenyl Benzoxazine (DCB) anti-corrosive agent (polymer synthesis) [23,24]

To prepare MS substrates for coating, they were mechanically blasted to Sa 2.1/2 and cleaned in acetone using ultrasonic technology. The polymer coating was applied to the MS plate using thermal curing and dip coating techniques. Before adding the isocyanate hardener (DCB-PU 60, DCB-PU 80, or DCB-PU 100) in equivalent amounts, the monomer (DCB) was dissolved in a solvent mixture (7:3 1,4-dioxime/toluene). The MS plate was then removed from the DCB solution at a steady rate of 100 mm per minute after being submerged in it for one minute. The DCB-coated MS samples underwent three rounds of the aforementioned technique. Subsequently, they were stored overnight at room temperature and then vacuum-dried for one hour at 100°C to remove any solvent molecules. Finally, the specimens were thermally treated at 180°C for three hours.

Water absorption studies [25]

The water absorption of cured coating samples was tested following the guidelines of ASTM D570. The samples were first dried in a vacuum oven at 80°C and then soaked in water at room temperature for a day. After removing the absorbed water, the samples were dried and weighed. Tissue paper was used to dye the samples. We confidently employed the following equation to ascertain the percentage of water absorption:

Percentage of water absorption = $[(W_a-W_b)/W_b]$ X 100

Where,

Wa = Weight of the cured sample after removal the exposure to water absorption

Wb = Weight of the cured sample before removal the exposure to water absorption

Gel content studies [25]

To determine the total gel content of the cured coating sample, we accurately weighed the bare coated sample and soaked it in xylene at room temperature for 24 hours. Afterwards, we dried the cured coating samples in a vacuum-sealed oven. To calculate the gel content of coated samples, we utilized the following equation:

Percentage of gel content = (W_a/W_b) X 100

Where Wa and Wb are the weight of cured coating samples after and before the extraction respectively.

Computational calculations

The DCB's frontiers molecular orbitals (FMO) of the monomer were investigated using density functional theory (DFT). The software used for these calculations is the Gaussian 09W software. For the monomer's structural optimization, the B3LYP/6.311 G basis set was applied. [26] In the theoretical UV-visible experiment, time-dependent DFT (TDDFT) and other fundamental techniques were employed. The Gauss view software was used for various further process such as three-dimensional visualization including FMO, electron clouds identification on the compound, molecular electrostatic potential (MEP) and Mullikan charge distribution representations.

Tafel Polarization experiment [27]

By aid of these values, the corrosion efficacy was calculated using following formulae,

Corrosion rate = (Icorr × K × EW)/ρAmmpy

Where, K is corrosion rate constant (K= 3272 mm $year^{-1}$),EW is equivalent weight of the MS (27.9 g), ρ is MS density (7.85 g cm^{-3}) and A is an area of the sample1 cm^2.

Corrosion Efficiency (%) = [(Icorr(b)-Icorr(c))/(Icorr(b))] × 100 Where, Icorr(b) is corrosion current values for the bare mild steel, Icorr(c) is corrosion current values for the material coated mild steel.

Results and discussion

FT-IR spectroscopic studies

FT-IR spectroscopy is a dependable method to obtain data on the unique vibrational frequency of each functional group in an organic molecule. The peaks have been identified in their respective ranges according to the bond polarity. Utilization of this spectroscopic technique is wide-spread thus includes organic, nano-particles, biomass. [28-29]Additionally, it offers a variety of applications that might be used to forecast the way that molecules interact in liquid form. [30-31] In Figure 1, the FT-IR spectra of the monomer are displayed. The peaks at 2929 and 2852 cm^{-1} are caused by aromatic stretching vibrations. Additionally, the cyclic amine functional group is associated with a high peak at 1197 cm^{-1} due to C-N stretching vibration. The peaks at 1254cm^{-1}, 1281cm^{-1}, and 1043 cm^{-1} indicate the presence of asymmetric and symmetric stretching vibrations of the C-O-C bond. A strong signal at 609 cm^{-1} indicated the presence of an ortho-substituted epoxy group, and a subsequent peak at 1471 cm^{-1} firmly established the existence of a tri-substituted benzene ring that has been fused with an oxazine ring. This study strongly supported the idea that the synthesised monomer has a specific functional group, in this case an aromatic group fused to an oxazine ring [32]. The polymeric composites also showed these

corresponding peaks, and additional notable peaks that relate to the vibrations of polyurethane were also seen. For instance, the very weak boarded peaks that were observed at 3378 cm^{-1} and 3142 cm^{-1}, respectively, are caused by the -NH- and -CH_2 stretching vibrations. The stretching vibrations of the C-N and C-O-C bonds, respectively, are associated to a series of high peaks at 1571cm^{-1} and 1129 cm^{-1}, which were also seen [33]. The presence of the polyurethane unit in the synthetic composites is thus confirmed by this encounter.

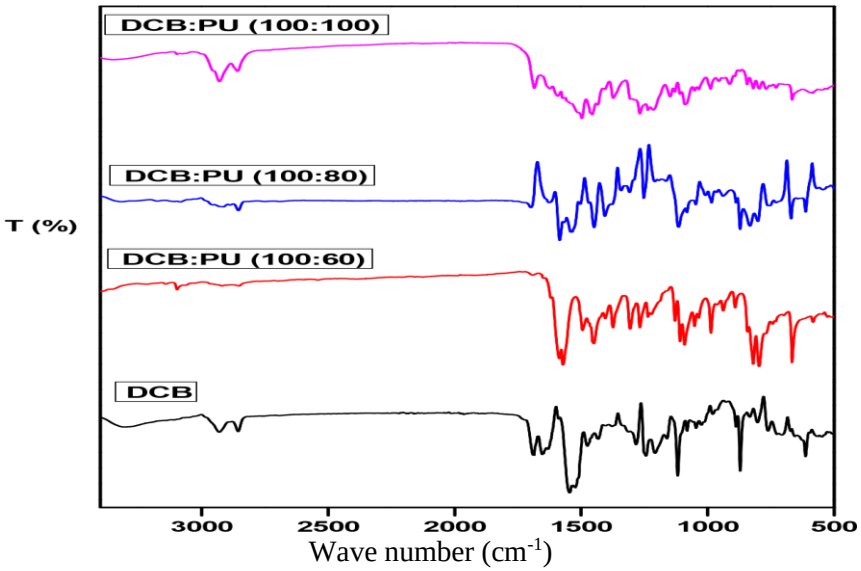

Figure 1: FT-IR spectra of the monomer and polymeric composites

NMR studies

NMR spectroscopy is one of the crucial instruments that can accurately detail each proton's precise chemical situation of the crucial instruments that can accurately detail each proton's precise chemical situation is NMR spectroscopy. The proton NMR analysis was used to describe the currently synthesized monomer. In Figure 2, a sharp and intense singlet peak at 2.15 ppm corresponding to the three protons were attributed to the methyl group attached in the aromatic ring. Next to that, a couple of singlet peak has obtained at 4.52 ppm and 5.25 ppm accounted for two protons of each. This is confirming that formation of heterocyclic via coupling reaction. The chlorinated aromatic three protons were found at 6.47 ppm, 6.65 ppm and 6.87 ppm as singlet peaks. Besides, the methyl group attached aromatic protons was involves spin-spin coupling leads to splitting of the peaks that can be find at the 6.47 ppm and 7.19 ppm as a multiplate. This observed peaks that clearly suggested that monomer formation during the synthesis.

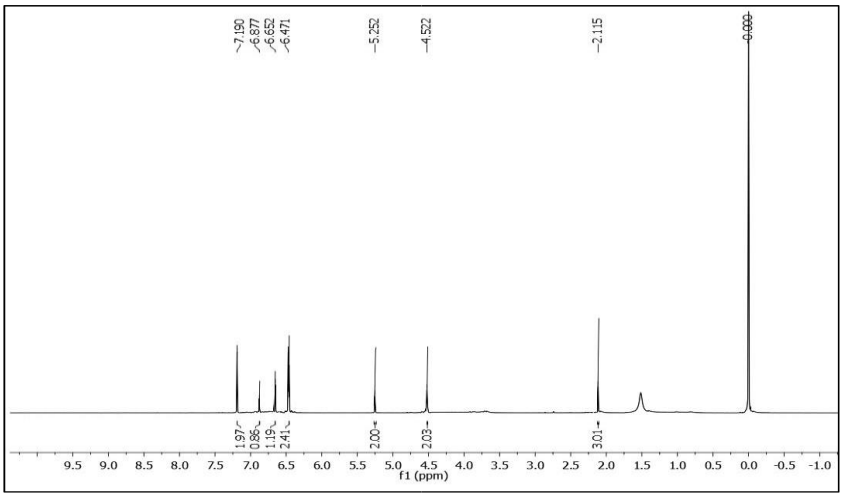

Figure 2: ^1H NMR-spectrum of the monomer in $CDCl_3$

UV-visible spectroscopy

The synthesised DCB and its polymers have been studied using UV-visible spectroscopy. The spectra were recorded at room temperature, and water was utilised as a solvent to dissolve the compounds. As seen in Figure 3, the synthesised monomer displays two peaks, one at 346 nm and the other at 298 nm. The first peak was obtained to broaden, and the latter peak was obtained as a high absorbance peak. These two peaks correspond to the n-π* and π - π * electronic transitions of the monomer. In a similar vein, polyurethanecoupled materials were also investigated. All polymeric materials have been resembled with monomers with increasing absorbance intensity with red shift. The gradual changes in the spectrum of monomer with polymeric composite reveals that the strong influences of the polyurethane unit in the both electronic transitions of the monomer. In particular n-π* transition band shifted towards higher wavelength of 20 nm with maximum polymeric content material with hike in the π - π * electronic transition leads to rigid band at 358 nm.

These findings demonstrate unequivocally that a significant amount of polyurethane has an impact on the monomer's own characteristics. Consequently, the predominance of polyurethane in the material contains 100 % polyurethane, may be advantageous for the application procedure.

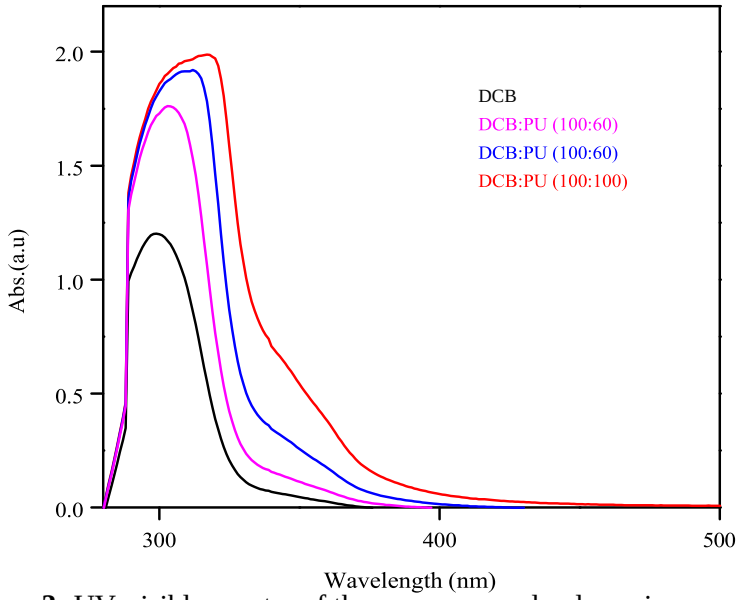

Figure 3: UV-visible spectra of the monomer and polymeric composites.

Electrochemical studies

The Tafel plot in Figure 4 was used to calculate the corrosion current and potential of the artificial polymeric material. Specifically, the corrosion potential was used to predict the corrosion current density by overlaying a straight line on the linear component of both the anodic and cathodic curves. These features greatly impact the corrosion behaviour of the synthesized materials. When the materials have increased conductivity and more electrons, the larger corrosion current usually speeds up corrosion. On the other hand, having a higher positive corrosion potential result in a lower corrosion rate. As a result, materials require a higher potential to display their conductivity. [34-35]

The data in Table 1 shows the tafel plot results for both blank and polymeric materials. The blank material had a higher Icorr value, meaning it corroded more than the polymeric materials. To prevent this, the mild steel was coated with three different polymers containing varying amounts of polyurethane. The polymers with higher polyurethane content were found to provide better corrosion inhibition. One particular material, which was 100% polyurethane, showed an Icorr in the pico ampere range, indicating it had low conductivity and high corrosion inhibition properties. It's possible that the reason for this is because of the creation of more cross-linkages, which makes the materials more hydrophobic and thus reduces corrosion. The blank's corrosion potential also showed a more negative value, indicating an easy oxidation behaviour that could be addressed quickly. The polyurethanecoated samples showed fewer corrosive characteristics and changed towards a positive potential. This was achieved up to 80% polymer coating, but the sample with 100% polymer coating once again showed a larger negative potential, despite having less corrosion current. It's been suggested that this aberrant behaviour may be caused by the oxidation

of monomeric material, which creates new polymeric forms. As the polyurethane content increases, other parameters such as the corrosion rate also decrease. Samples coated with 60% polyurethane have an impressively high efficacy of 99.5% in preventing corrosion. Interestingly, coating the samples with 100% polyurethane only marginally improves this efficacy. Finally, it has been observed that samples coated with polyurethane have exhibited anti-corrosion properties. Therefore, it is possible that this material could serve as a more efficient inhibitor of mild steel corrosion.

Table 1: Data obtained from the tafel experiments

S. No	Samples	Corrosion Current (nA)	Potential (mV)	Cathodic slope (mV/dec)	Anodic slope (mV/dec)	Corrosion rate (mm/year)	Corrosion inhibition efficacy (%)
1	Blank	601	-839.00	-43.10	39.10	6989113.44	0.00
2	60:100	2.77	-751.00	-46.00	37.10	32212.71	99.53
3	80:100	1.38	-793.00	-44.00	47.70	16048.21	99.77
4	100:100	0.00119	-865.00	-56.30	50.90	13.83	99.99

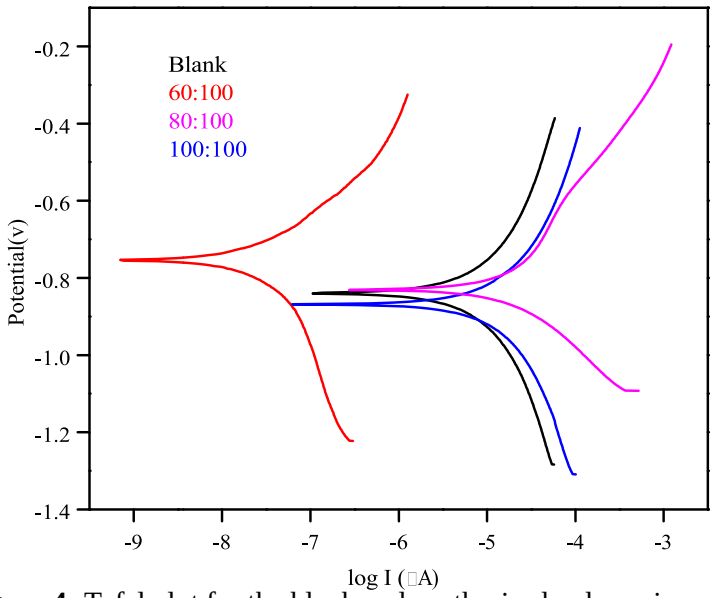

Figure 4: Tafel plot for the blank and synthesised polymeric materials

Microscopic optical imagic studies

Through the analysis of optical images, one can observe the anti-corrosive effects of a coated polymer. Figure 5 serves to showcase how the concentration of the polymer material has a direct impact on the coating. Any morphological damage on the surface will be easily visible as a dark red tone when exposed to light. The study delves into the application of coatings on polymeric composites, which are known to have weak and ineffective anticorrosive properties. Despite the mild having a 60% loaded material coating, it has eroded almost completely. However, the fact that a small amount does not appear red is indicative of its anti-corrosive properties. Moreover, the corrosion was effectively suppressed by the addition of higher polyurethane content (100%). This did not alter the colour of the surfaces that were only slightly affected.

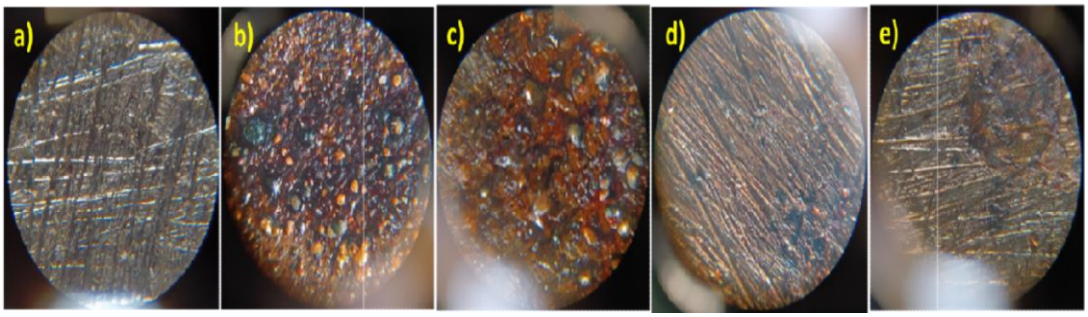

Figure 5: Optical microscopic images of the before corrosion, after corrosion (b) only monomer, (c) DCB/PU (100-60), (d) DCB/PU (100-80) and (e) DCB/PU (100-100)

Water absorption and gel content studies

It is generally known that studies on water diffusion in polymeric corrosion materials are very essential and can depend on the branching and cross linkage density of the polymeric materials. The effectiveness of the binder during coating is determined by the density of the cross or breach, which can give better hydrogen bonding with the materials.[36] The water absorption capacity of the all-synthesized monomer and polymeric compounds have seen in figure 6. Results clearly indicates that DCB having more water absorption as compared to the polymeric materials. DCBshows the percentage of water absorption is 1.8 whereas 60 % polymer loaded material gets down to the 1%. At the maximum loaded polyurethane has reached to 0.7 % thus due to more cross linkage in the compound have makes more hydrophobic nature of the whole compound. This is strongly repelling the water molecules. These characterizations of the polymeric material have been realized could be anti-corrosive properties. Similarly, gel content of the synthesized monomer and its polymeric materials has been studies because of its structural importance. Figure 7 shows the calculated data obtained from the experimental studies. DCB itself shows 85.2 % gel content thus reveals that more gel formation feasibility of monomer. Up on the addition of polymeric content to the monomer leads to increase the gel content thus 60 % polymer content has been strengthening the gel formation up to 89.1 %. This can be improved by adding more polymeric content which shows almost 94 % gel content that is 10 point higher than the monomer. This might be attributed to the proper interaction between polyurethane unit and monomeric unit.

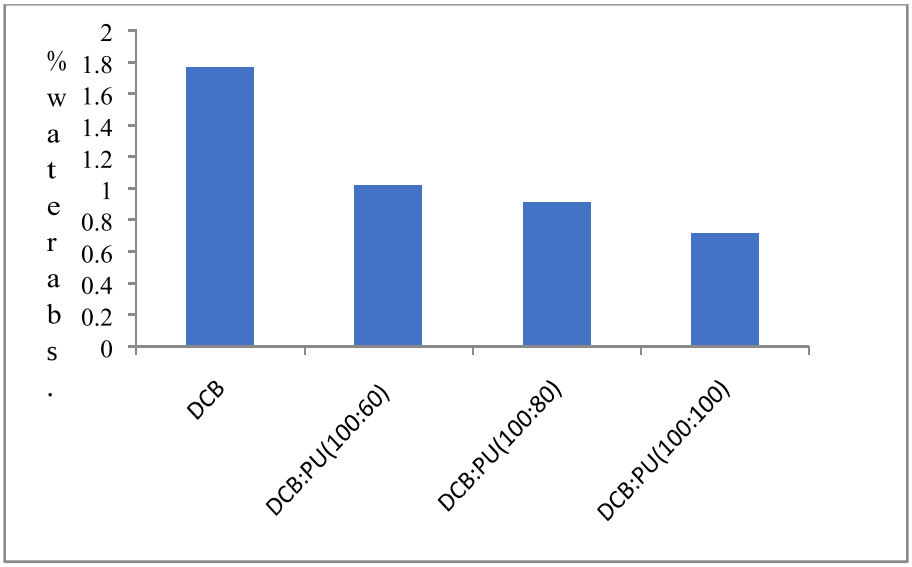

Figure 6: Water absorbance studies of the DCB and its polymeric composites

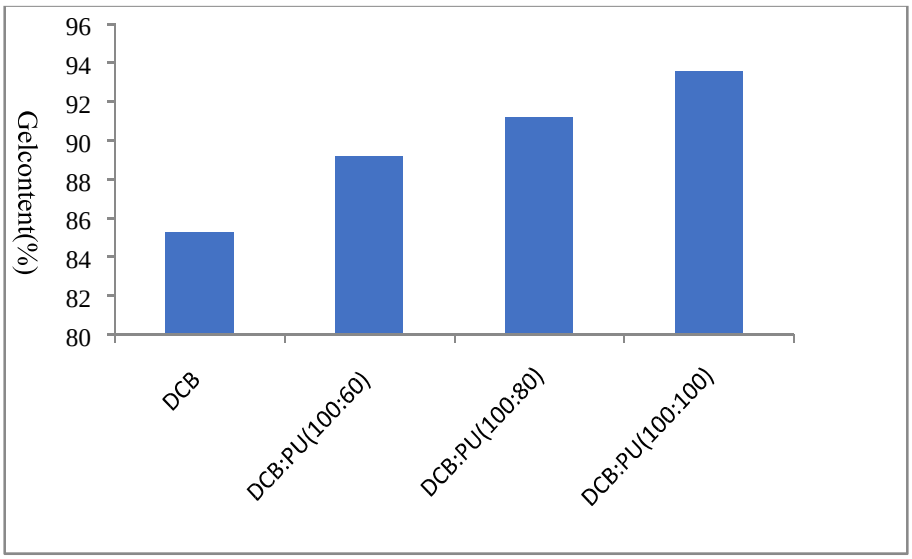

Figure 7: Determination of the gel content in the DCB and its polymeric composites

DFT analysis

It is an extremely crucial theoretical approach that can be used in a wide range of research fields, including OLED, solar cells, chemo-sensors, catalysis, biological applications, etc. [37-40] In this investigation compound's structural and electronical properties have been revealed, are particularly needed to support research in the drug discovery process. This might make it easier to determine how chemically reactive the substance is with regard to biomolecules. Several compound properties, including chemical reactivity, global hardness, global softness, and electrophilicity index, have been quantified solely using this method. So, this work has also been incorporated in the current studies. Although LUMO designates the lowest vacant molecular orbital, HOMO refers to the highest occupied molecular orbital. Frontier molecular orbitals (FMOs) refer to both HOMO and LUMO, and Figure 8 shows the FMO of the synthesized DCB.In HOMO, the electrons were located at aryl amine and benzoxazole moieties. The electron cloud has been completely shifted to the aryl amine ring at LUMO level; this charges transformation is attributed to the presence of two chloride atom present in the aryl ring at meta position that act as electron withdrawing group. The presence of intra molecular charge transfer reveals that compound having more polarity which may help in the making various cross links during the polymerization reaction. The value of the FMO's is given in the table 2; the compound has obtained HOMO and LUMO values of -5.9132eV and -0.6081 eV. These values are used to calculate various parameter which is supports to the compound's chemical reactivity such as global softness, global hardness, chemical potential and electronegative index. The energy band gap value also calculated that has obtained to be 5.3051 eV which is responsible for the
observed transition in UV-visible spectroscopy (233.7 nm). The obtained above mentioned parameter values are displays that an excellent reactivity of the compound.

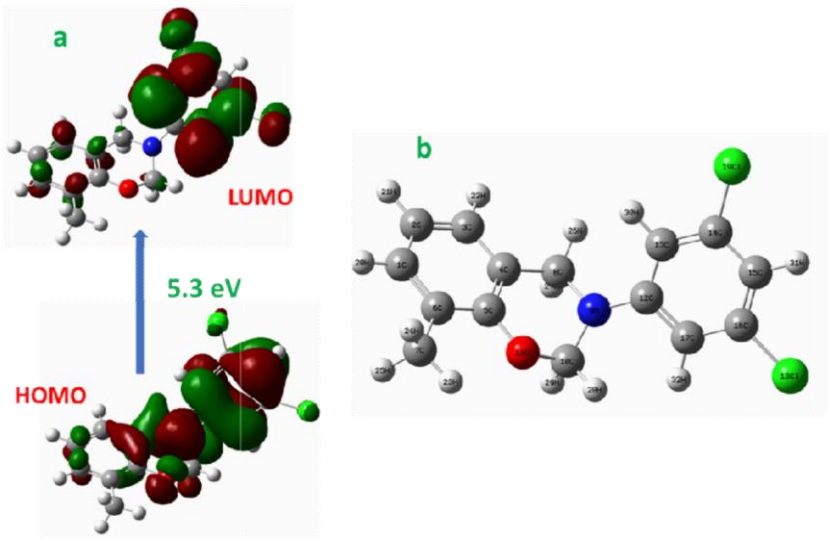

Figure 8: FMO analysis of the synthesized DCB and its optimized structure

Table 2: Parameters calculated from DFT studies.

Compound name	HOMO (eV)	LUMO (eV)	Band gap (□E)	Chemical potential	Global hardness	Global softness	Electrophilicity index
C-Bz	-5.9132	-0.6081	5.3051	-3.2607	- 2.6525	-0.1884	-2.0041

Molecular Electrostatic Potential (MEP)

Data on molecular electrostatic potential were obtained by several reliable quantum chemical processes. This research could be extremely beneficial and be applied to understanding and predicting the chemical reactivity of molecules. [41] Using this technique, the compound's three-dimensional structure has been shown through the dispersion of electronic charges. Thus, it could be beneficial to simply analyses the charges of the entire molecule. This study helps to visualize the molecule's electron sink or surface by colours. [42] Typically, three colours are used to represent the compound's surface's electrical density. Strong red colour denotes more electron-rich, whereas green colour denotes the area that is more positively charged and symbolizes the area that is electron-poor. The neutral charge of the compounds has

been indicated by the colour blue, making it simple to understand the electronic charge by mapping the surface. Hence, will make crystalline decisions on the molecules' reactivity.The successive studies of the DFT, MEP also carried out using the optimized structure derived from the DFT analysis. A strong red colour on oxygen of the benzoxazole ring reveals high electro negative region of compound thus due to presence of lone pair electrons. Next to that, a weak electro negativity of compound has arisen on the chloride atoms of the aryl ring shows as yellow colour. This is also verified from the DFT studies inducing intra molecular charge transfer. A shadow of blue colour was obtained at the nitrogen region of the benzoxazole ring respectively for more electron deficient region and other aromatic carbons are showing green colour means that neutral charges. However, particularly nitrogen atom hasn't shown any blue color thus clearly indicates that nitrogen is not being electropositive atom in this molecule. Overall, the synthesized new monomer having both electron rich and deficient region which is also supports for ICT process. Moreover, this could be making more electrostatic and hydrophobic interactions during the polymerization process which is strengthen for the corrosion studies.

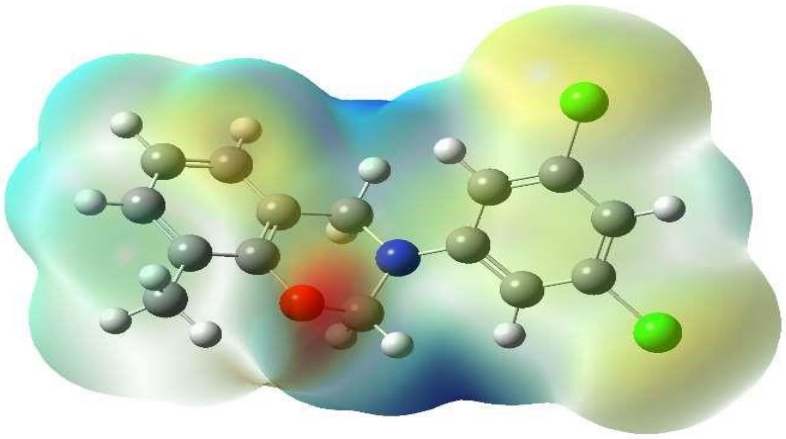

Figure 9: Molecular electrostatic potential analysis of the synthesized monomer

Mullikan's charge distribution

This method is the most highly detailed compared to the other ways discussed above. This method accounts for the precise value of charges on each atom, whereas the earlier one only offers the general charge distribution. Since the obtained charges of the atoms are partial and depend on the linear combination of atomic orbitals, the 3D structure of the organic ligands was determined for this purpose from the output file of DFT investigations. The importance of this topic is therefore unavoidable and is a crucial component of ligand and biomolecular interactions. Additionally, the bond's strength during biomolecule contact can be calculated based on the individual charges of the atoms included in a given bond. As a result, it provides a ready-made toolkit for identifying the atom that would be best for interactions with biomolecules like hydrogen bonds. Consequently, simplifying the understanding of the ligand's structural characterisation during the biomolecular interaction [43-44].

Hence, the synthesized DCB has been analyzed further for mullikan's charge distribution. The charge distribution of each atom is presented in bar chat and its optimized structure also shown in Figure 10. The quantified electronic charges of the monomer show three atoms which having more negative charges that are cresol methyl carbon, benzoxazole nitrogen and oxygen. Additionally, chlorine attached carbon atoms of aryl amine ring also show significant negative charges. Further, the oxygen and nitrogen attached carbons of benzoxazole ring acquired more positive charges due to electro negativity of hetero-atoms. Other, atoms like hydrogens are obtained limited positive charges which is also due to electronegative difference of carbon and hydrogen atom. This studies also conclude that all charges (positive, negative and neutral) were spread over the molecule which can be helps to make better bonding interaction during the polymerization.

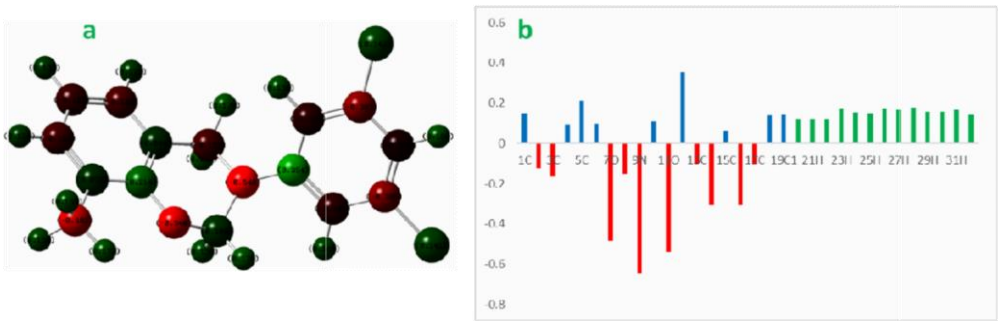

Figure 10: (a) Mullikan's charge distribution of the synthesized monomer and (b) quantified data of each atom present in the bar chat.

Conclusion

O-cresol serves as the fundamental structure of a newly synthesized heterocyclic benzoxazole-based monomer. The FT-IR, NMR, and UV-visible spectroscopy approaches were used to further characterize this monomer, and the results supported its chemical structure. Additionally, the polymeric composites made from the monomer, which were synthesized using polyurethane, were utilized to study the monomer's ability to suppress corrosion. By using FT-IR and UV-visible spectroscopy, three distinct ratios of monomer and polyurethane composites were identified. The corrosion results demonstrate that materials with a higher polyurethane content have more successfully inhibited corrosion than other materials. The polymers' ability to absorb water and the presence of a significant percentage of gel content account for their corrosion prevention properties. The optical microscopic imaging tests have shown the effects of the polymer coating on steel, which greatly aids the tafel experiments. Additionally, DFT investigations such as FMO's analysis, MEP, and Mullikan's charge distribution have shown the monomer's chemical reactivity. According to all investigations, monomer and its polymeric composites had a significant influence on studies of mild steel corrosion.

References

1. A. Alamiery, Anti-corrosion effect of thio-semicarbazide derivative on mild steel in 1M hydrochloric acid and 0.5 M sulfuric Acid: Gravimetrical and theoretical studies Materials Science for Energy Technologies 4, 2021, 263
2. Salc, H. Yüksel, R. Solmaz Experimental studies on the corrosion inhibition performance of 2-(2-aminophenyl) benzimidazole for mild steel protection in HCl solution Journal of the Taiwan Institute of Chemical Engineers 134, 2022, 104349
3. G. Schmitt, M. Schütze, G.F. Hays, W. Burns, E. Han, A. Pourbaix, G. Jacobson, Global Needs for Knowledge Development in Materials Deterioration and Corrosion Control in cooperation with, Fed. Highw. Adm. FHWA-RD-01 (2009) 1.
4. M. Jaishankar, T. Tseten, N. Anbalagan, B. B. Mathew, and K. N. Beeregowda Toxicity, mechanism and health effects of some heavy metals Interdiscip Toxicol. 7, 2014, 60.
5. C. Kingsley, R. Uche, O. C. Nwufo Effect of Corrosion on Mild Steel in Food Processing Industry: A Review International Journal of Advanced Engineering Research and Science, 9, 2022
6. S. B. Ulaeto, R. P. Ravi, I. I. Udoh, G. M. Mathew, T. P. D. RajanPolymer-Based Coating for Steel Protection, Highlighting Metal–Organic Framework as Functional Actives: A Review Corros. Mater. Degrad. 4, 2023, 284
7. A. Singh, M. Liu, E. Ituen, Y. Lin Anti-Corrosive Properties of an Effective Guar Gum Grafted 2-Acrylamido-2-Methylpropanesulfonic Acid (GG-AMPS) Coating on Copper in a 3.5% NaCl Solution Coatings 10, 2020, 241
8. H. R. Obayes, G. H. Alwan, A. H. M. Alobaidy, A. A. Al-Amiery, A. A. H. Kadhum, A. B. Mohamad, Quantum chemical assessment of benzimidazole derivatives as corrosioninhibitors, Chem. Central J. 8, 2014, 21.
9. S. Junaedi, A. Al-Amiery, A. Kadihum, A. Kadhum, A. Mohamad, Inhibition effects of a synthesized novel 4-amino-antipyrine derivative on the corrosion of mild steel in hydrochloric acid solution together with quantum chemical studies, Int.J.Mol.Sci.14, 2013, 11915.
10. S. Kumari, A. Saini, V. Dhayal Metal oxide-based epoxy coatings for corrosion protection of steel material today: proceedings 43, 2021, 3105

11. Verma, L. Olasunkanmi, E. D. Akpan, M. A. Quraishi, O. Dagdag, M. E. Gouri, E-S. M. Sherif, E. E. Ebenso, Epoxy resins as anticorrosive polymeric materials: A review Reactive and Functional Polymers 156, 2020, 104741
12. A.S. Castela, A.M. Simões, An impedance model for the estimation of water absorption in organic coatings. Part I: A linear dielectric mixture equation, Corros. Sci. 45, 2003, 1631
13. W.-G. Ji, J.-M. Hu, L. Liu, J.-Q. Zhang, C.-N. Cao, Water uptake of epoxy coatings modified with γ-APS silane monomer, Prog. Org. Coat. 57, 2006, 439
14. S. Jamshidia, H. Yeganeha and S. Mehdipour-Ataei Poly(urethane-co-benzoxazine)s via reaction of phenol terminated urethane prepolymers and benzoxazine monomer and investigation of their properties Polym. Adv. Technol. 22, 2011, 1502
15. J. R. Oliveira, L. R. V. Kotzebue, D. B. Freitas, A. L. A. Mattos, A. E. da Costa Júnior, S. E Mazzetto. Towards novel high-performance bio-composites: polybenzoxazine-based matrix reinforced with Manicariasaccifera fabrics. Compos B Eng 194, 2020, 108060
16. Peng, Z. Wu, D. Zhou. Synthesis of a benzoxazine-type dispersant and its application on epoxy/benzoxazine/ZrO_2 composite: dispersion performance and tensile behavior. Compos B Eng 167, 2019, 507
17. A. M. M. Soliman, K. I. Aly, M. G. Mohamed, A. A. Amer, M. R. Belal, M. AbdelHakim Synthesis, characterization and protective efficiency of novel polybenzoxazine precursor as an anticorrosive coating for mild steel Sci Rep. 13, 2023, 5581.
18. T. F. Cummings, J. R. Shelton Mannich Reaction Mechanisms J. Org. Chem., 25, 1960, 419
19. P. A. Sørensen, S. Kiil, K. Dam-Johansen C. E. Weinell Anticorrosive coatings: a review Journal of Coatings Technology and Research 6, 2009, 135
20. M. A. Petrunin Advances in Anti-Corrosion Polymeric and Paint Coatings on Metals: Preparation, Adhesion, Characterization and Application Metals, 12, 2022, 1216
21. T. Krucker, A. Lang, E. P Meyer New polyurethane-based material for vascular corrosion casting with improved physical and imaging characteristics Microsc Res Tech. 69, 2006, 138
22. H. Wang, J. Xu, X. Du, Z. Du, X. Cheng, H. Wang A self-healing polyurethane-based composite coating with high strength and anti-corrosion properties for metal protection Composites Part B: Engineering 225, 2021, 109273
23. C. Zhou, X. Lu, Z. Xin, J. Liu, Y. Zhang Hydrophobic benzoxazine-cured epoxy coatings for corrosion protection, Progress in Organic Coatings 76, 2013, 1178
24. X. Lu, Y. Liu, C. Zhou, W. Zhanga, Z. Xin Corrosion protection of hydrophobic bisphenol A-based polybenzoxazine coatings on mild steel RSC Adv., 6, 2016, 5805
25. K. Jayanthi, M. Sivaraju, P. Shanmugasundaram Enhancing Corrosion Resistance Property of Mild Steel by Benzoxazine Synthesized from Vanillin and Copolymerize with UrethaneVol. 35, No. 4 (2023), 851-860
26. R. Kavitha, S. Nirmala, R. Nithyabalaji, R. Sribalan Biological evaluation, molecular docking and DFT studies of charge transfer complexes of quinaldic acid with heterocyclic carboxylic acid 1204, 2020, 127508
27. G. A. Phalak, D. M. Patil, S.T. MhaskeSynthesis and characterization of thermally curable guaiacol based poly(benzoxazine-urethane) coating for corrosion protection on mild steel European Polymer Journal, 88, 2017, 93
28. A Senthil Murugan, N Vidhyalakshmi, U Ramesh and J Annaraj In vivo bio-imaging of sodium meta-arsenite and hydrogen phosphate in zebrafish embryos using red fluorescent zinc complex Sensors and Actuators B: Chemical 281, 2019, 507
29. A. Senthil Murugan, D Singh, S Mahala, B Devi, S Kumar, S Jakhu and S Elumalai MgO/CaO Nanocomposite Facilitates Economical Production of d-Fructose and dAllulose Using Glucose and Its Response Prediction Using a DNN Model Industrial & Engineering Chemistry Research 61, 2022, 2524.
30. S. Kumar, S. Sharma, S. M. Arumugam, C. Miglani, S. Elumalai Biphasic separation approach in the DES biomass fractionation facilitates lignin recovery for subsequent valorization to phenolics ACS Sustainable Chemistry & Engineering 8, 2021, 19140
31. A. Senthil Murugan, N Vidhyalakshmi, U Ramesh, J Annaraj A Schiff's base receptor for red fluorescence live cell imaging of Zn^{2+} ions in zebrafish embryos and naked eye detection of Ni^{2+} ions for bio-analytical

applications Journal of Materials Chemistry B 5, 2017, 3195
32. M. M. Hussein, S. A. Saafan, N. A. Salahuddin, M. K. Omar Polybenzoxazine/Mg– Zn nano-ferrite composites: preparation, identifcation, and magnetic properties Applied Physics A 127, 2021, 488
33. S. Caddeo, F. Baino, A. M. Ferreira, S. Sartori, G. Novajra, G. Ciardelli, C. V. Brovarone Collagen/Polyurethane-Coated Bioactive Glass: Early Achievements Towards the Modelling of Healthy and Osteoporotic Bone Key Engineering Materials. 631, 2015, 184
34. C. Zhou, X. Lu, Z. Xin, J. Liu and Y. Zhang, Hydrophobic benzoxazine-cured epoxy coatings for corrosion protection, Prog. Org. Coatings. 76, 2013, 1178.
35. D. Prasai, J.C. Tuberquia, R.R. Harl, G.K. Jennings and K.I. Bolotin, Graphene: Corrosion-inhibiting coating, ACS Nano. 6, 2012, 1102
36. G. A. Phalak, D. M. Patil, S.T. Mhaske Synthesis and characterization of thermally curable Guaiacol based poly (benzoxazine – urethane) coating for corrosion protection on mild steel 88, 2017, 93
37. S. Kumar, S. M. Arumugam, S. Sharma, S. Mahala, B. Devi, S. Elumalai Insights into the kinetics and mechanism of spermine (base)-catalyzed D-fructose interconversion to low-calorie D-allulose Molecular Catalysis 533, 2022, 11275
38. A. Senthil Murugan, M. Kiruthika, E. R. A. Noelson, P. Yogapandi, J. Annaraj Fluorescent sensor for in-vivo bio-imaging, precise tracking of Fe3+ ions in Zebrafish embryos and visual measuring of Cu2+ ions in pico-molar level Arabian Journal of Chemistry 14, 2021, 102910
39. S. S. Nishat, Md. J. Hossain, F. E. Mullick, A. Kabir, S. Chowdhury, S. Islam, M. Hossain Performance Analysis of Perovskite Solar Cells Using DFT-Extracted Parameters of Metal-Doped TiO_2 Electron Transport Layer J. Phys. Chem. C 125, 2021, 13158
40. R. Zaiera, S. Hajajia, M. Kozakib, S. Ayach DFT and TD-DFT studies on the electronic and optical properties of linear π-conjugated cyclopentadithiophene (CPDT) dimer for efficient blue OLED Optical Materials 91, 2019, 108
41. H. Suresh, G. S. Remya, P. K. Anjalikrishna Molecular electrostatic potential analysis: A powerful tool to interpret and predict chemical reactivity Wiley Interdisciplinary Reviews: Computational Molecular Science. 2022 (https://doi.org/10.1002/wcms.1601)
42. S. Lakshminarayan, V. Jeyasingh, K. Murugesan, N. Selvapalam, G. Dass Molecular electrostatic potential (MEP) surface analysis of chemo sensors: An extra supporting hand for strength, selectivity & non-traditional interactions Journal of Photochemistry and Photobiology 6, 2021, 00022
43. R. S. Mulliken, Electronic Population Analysis on LCAO–MO Molecular Wave Functions. I, J. Chem. Phys. 23, 1955, 1833-1840.
44. S. Madhankumar, P. Muthuraja and M. Dhandapani, Structural characterization, quantum chemical calculations and Hirshfeld surface analysis of a new third order harmonic organic crystal: 2-Amino-4-methylpyridinium benzilate, J. Mol. Struct. 1201, 2020, 127151